

Spin Rotations in a Bose-Einstein Condensate Driven by Counterflow and Spin-Independent Interactions

David C. Spierings¹,* Joseph H. Thywissen¹, and Aephraim M. Steinberg¹
Department of Physics and CQIQC, University of Toronto, Toronto, Ontario M5S 1A7, Canada

 (Received 31 August 2023; accepted 13 March 2024; published 23 April 2024)

We observe spin rotations caused by atomic collisions in a nonequilibrium Bose-condensed gas of ^{87}Rb . Reflection from a pseudomagnetic barrier creates counterflow in which forward- and backward-propagating matter waves have partly transverse spin directions. Even though inter-atomic interaction strengths are state independent, the indistinguishability of parallel spins leads to spin dynamics. A local magnetodynamic model, which captures the salient features of the observed spin textures, highlights an essential connection between four-wave mixing and collisional spin rotation. The observed phenomenon is commonly thought not to occur in Bose condensates; our observations and model clarify the nature of these effective-magnetic spin rotations.

DOI: [10.1103/PhysRevLett.132.173401](https://doi.org/10.1103/PhysRevLett.132.173401)

Spin dynamics in cold atomic gases exhibit rich phenomena due to the interplay of particle interactions, quantum coherence, and particle statistics. In a Bose-Einstein condensate (BEC) with only contact interactions, spin dynamics can be induced by the spin dependence of the interaction strengths between particles. If interspin and intraspin interaction strengths are the same, on the other hand, there is only one scattering length, a . When all atoms have the same kinetic energy and experience the same trapping potential regardless of spin, one might be tempted to conclude that all spin components have the same energy and therefore distribute themselves evenly following the density profile.

Wavelike spin excitations (i.e., spin waves), however, have long been known to arise in Fermi gases and *non-degenerate* Bose gases even in the absence of spin-dependent interactions [1–4], and have been observed in a variety of systems [5–13]. Spin waves in dilute quantum gases are generated by the identical-spin rotation effect (ISRE), an effective magnetic interaction in which colliding spins precess about their net spin [11,14,15]. Both ISRE and the closely related Leggett-Rice effect [16] arise from the interaction energy difference when two identical particles collide with their spins aligned or anti-aligned due to exchange-symmetry contributions. Particle exchange modifies the interaction energy of a gas by $g\rho$, for particle density ρ and spin-independent interaction strength $g = 4\pi\hbar^2 a/m$. In contrast, all particles in a BEC at zero temperature occupy the same single-particle state and so the many-body wave function can be written as one already-symmetrized product of single-particle wave functions (i.e., Hartree form), devoid of exchange contributions or bunching [17,18]. Combining these two statements has led to a widespread impression in the community that spin

rotations between identical particles do not occur in a condensate.

In this Letter, we observe spin dynamics emerging in a BEC that is reflected from a pseudomagnetic barrier. Counterpropagating matter waves generate a density modulation that leads to spin-dependent four-wave mixing, which we show can also be recast as an effective-magnetic spin rotation, whether or not the system is degenerate. This equivalence arises because a two-body interaction term $\hat{a}_{+k,\downarrow}^\dagger \hat{a}_{-k,\uparrow}^\dagger \hat{a}_{-k,\downarrow} \hat{a}_{+k,\uparrow}$ can be seen as either the exchange of momentum between two spins or the exchange of spin between two momentum modes.

Here we follow the latter picture and derive a magnetic interaction when the position is coarse-grained over a length scale much longer than that of the density modulation π/k , such that the local density can be approximated as constant. In this case, the populations of momentum components $+k$ and $-k$ are conserved locally. Remarkably, it follows [19] that pseudospin-half bosons with two such momenta experience an effective magnetic interaction given by

$$\begin{aligned}\dot{\vec{\sigma}}_{+k}(\mathbf{r}) &= g\rho_{-k}(\mathbf{r})\vec{\sigma}_{-k}(\mathbf{r}) \times \vec{\sigma}_{+k}(\mathbf{r}), \\ \dot{\vec{\sigma}}_{-k}(\mathbf{r}) &= g\rho_{+k}(\mathbf{r})\vec{\sigma}_{+k}(\mathbf{r}) \times \vec{\sigma}_{-k}(\mathbf{r}),\end{aligned}\quad (1)$$

where $\vec{\sigma}_{\pm k}(\mathbf{r})$ are position-dependent Bloch vectors for the $\pm k$ modes, and $\rho_{\pm k}(\mathbf{r})$ are the average densities of each momentum mode, summed over spin states. In this local magnetodynamic (LMD) model, the Bloch vector of each momentum mode rotates about the Bloch vector of the other, with a precession frequency determined by the counterpropagating mean field, $g\rho$.

In condensates with counterflow, the bosonic bunching observed in thermal systems is not present and the

nonequilibrium system can still be expressed in Hartree form. Nonetheless, for identical spins, there are density fluctuations due to interference. In both cases, the particle-particle correlations lead to increased interaction energy. Unlike ISRE, the spin-dependent dynamics arising from four-wave mixing persist into the mean-field limit and can be captured by a Gross-Pitaevskii (GP) treatment. Interfering particles see a higher average density because they spend more time near the peaks of the density distribution. By comparison, the orthogonally polarized component of the counterflow has a spatially uniform probability density. Hence, the interaction energy is different for the two spin states. This difference can be on the order of the energy of an entire condensate, since it includes contributions from all pairs of atoms, just as in the case of fragmentation [20,21]. The indistinguishability of particles permits both interference and exchange effects like ISRE.

Spatially inhomogeneous dynamics of two-component BECs has been studied in systems where component separation is created via the trapping potential [22,23] or induced by differences in interaction strengths [24,25]. Furthermore, component separation has been used as a mechanism for spin squeezing via the one-axis twisting Hamiltonian for systems with nearly equal interaction strengths [26–29]. Yet, the effective magnetic interaction typically ascribed to ISRE has not been directly observed in a condensed system, even though self-rephasing, a by-product of this interaction, has [30,31].

We study the generation of spin textures in a BEC of ^{87}Rb atoms in the $m_F = 0$ “clock” states of the $F = 1$ and $F = 2$ ground-state hyperfine manifolds, where F is the total angular momentum. This system can be conceptualized as a pseudospin-half system, where $|2, 0\rangle \equiv |+x\rangle$ and $|1, 0\rangle \equiv |-x\rangle$ [Figs. 1(a) and 1(b)]. Thanks to a coincidence of scattering lengths in ^{87}Rb , atom-atom interactions can be treated as spin-independent [32]. The experimental setup has been described in detail previously [33,34]. Typically, 3×10^3 atoms in a nearly pure condensate are prepared in $|x\rangle$ with a rms velocity width reduced to ≈ 0.3 mm/s via delta-kick cooling. Atoms are accelerated by a variable-duration magnetic-field gradient, and guided by a 1054 nm optical beam to preserve quasi-1D motion along the y axis. Typical clouds have a peak chemical potential $\mu/h = 50$ Hz, kinetic energy $E_k/h = 1.7$ kHz (velocity 3.9 mm/s), and cloud length 120 μm .

As illustrated in Fig. 1(c), the atoms encounter, and are partially reflected from, a barrier. The barrier is a 421.38 nm beam of light that has a Gaussian profile with $1/e^2$ radius of 1.3 μm along the y direction. It is overlapped by a pair of resonant Raman beams which act as a pseudomagnetic field localized to the barrier region and pointing along the z axis of the Bloch sphere [see Fig. 1(b)]. Hence, reflection generates a counterpropagating matter wave whose spin is rotated to an extent controlled by the Raman Rabi frequency Ω_B . These reflected atoms must

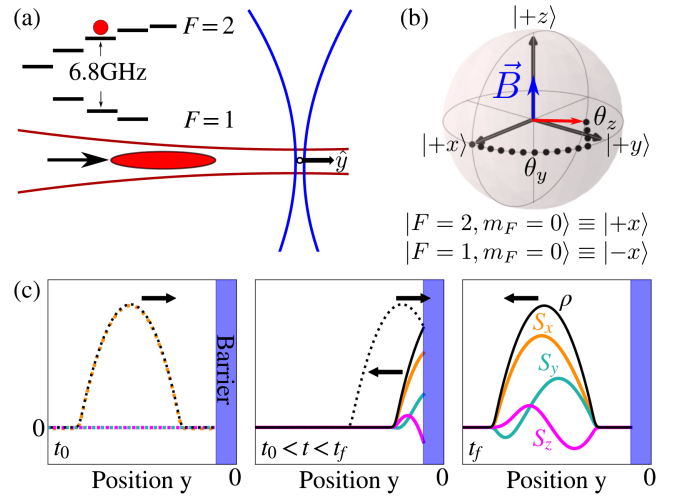


FIG. 1. Experimental configuration. (a) Illustration of the quasi-1D scattering configuration for the two-component BEC. (b) Bloch sphere representation of the magnetization of the BEC and the pseudomagnetic field \vec{B} within the barrier. (c) Spin rotation, S_x (orange), S_y (green), and S_z (magenta), during collision of right-going (dashed curves) and left-going (solid curves) atomic density (black), generated in reflection from a barrier that also acts as a magnetic field. Initially, at $t = t_0$, the spin of the right-going wave packet is polarized along $|+x\rangle$. Later, reflection from the barrier generates a left-going wave packet whose spin, not parallel with that of the right-going wave, rotates about the right-going spin (backaction on the right-going spin is not illustrated for simplicity). After complete reflection, at $t = t_f$, a spin texture is evident across the left-going density.

then propagate through the rest of the condensate, and collisions occur between reflected and incident atoms. These collisions are observed to have a significant effect, whereas in the previously studied case of transmitted atoms [33,34], they could be neglected. The phenomenon at the heart of our study is the counterflow spin dynamics, in which left-going spin rotates about right-going spin and vice versa. Note that the Raman beams are implemented using the same spatial mode as the barrier, through a combination of phase modulation at the clock frequency and attenuation of unwanted sidebands.

After the wave packet has left the barrier region, spin tomography is performed through a combination of sequential absorption imaging of the $|\pm x\rangle$ populations and a microwave pulse to rotate the axis of interest onto this measurement basis [34]. Spin profiles are extracted by computing the difference in the measured atom number in each absorption image pixel by pixel, integrating along the perpendicular direction, and dividing by the total reflected atom number. We report $S_i(y) = \int dx dz \sigma_i(\mathbf{r}) \rho(\mathbf{r}) / N_r$, where σ_i is the i th component of the Bloch vector of the cloud, and N_r is the total reflected atom number. We also report the aggregate rotation angles: θ_y describes the precession angle in the $S_x - S_y$ plane, and θ_z describes rotation out of that plane, resulting from the preferential

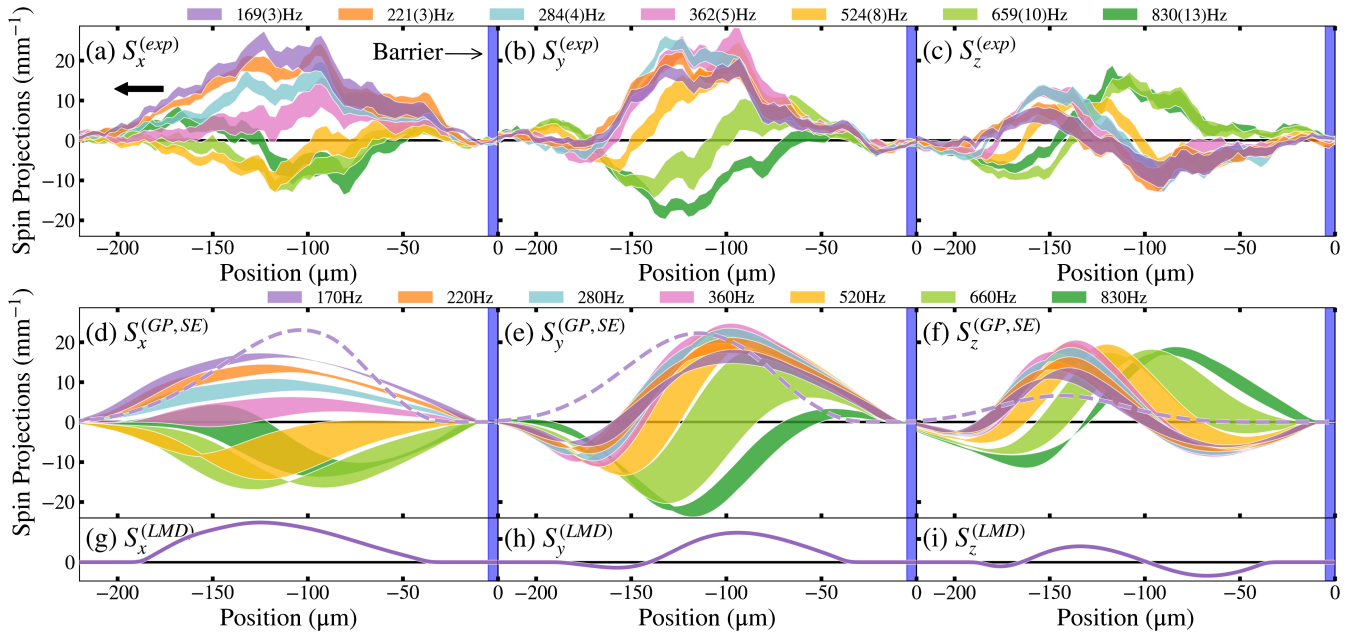


FIG. 2. Observed spin textures. S_x (left), S_y (middle), and S_z (right) spatial profiles for the reflected atomic cloud for various Ω_B (denoted by color). The atomic cloud, with mean incident energy of 1.67(5) kHz and rms energy width of 0.30(3) kHz, scattered from a barrier, located at the origin, with peak energy of 2.25(9) kHz. (a)–(c) Measured spin profiles with the bands representing 1 standard error in either direction from the average profile of the dataset. (d)–(f) Spin profiles predicted by GP simulations of the experiment. The shaded regions are bounded by simulations including 1 standard error in the measured barrier height and velocity width. The dashed line shows the predicted spin profile without atomic interactions for $\Omega_B/2\pi = 170$ Hz. (g)–(i) Predictions of the LMD model at $\Omega_B/2\pi = 170$ Hz for the average reflected velocity of this dataset.

reflection of the $|+z\rangle$ spin component which experiences an effectively higher barrier because it is parallel to the pseudomagnetic field [35].

Figures 2(a)–2(c) show the spin profiles observed in the reflected cloud for a BEC incident with average energy well below the barrier height, V_B . For these data, $\sim 95\%$ of atoms are reflected. Because the magnetic barrier has a spin-dependent transmission, the reflected cloud is partially polarized along $+z$. In the absence of interactions, this polarization direction would be essentially constant across the cloud. A billiardlike picture of elastic collisions could allow the spin to be redistributed spatially, but would never lead to local polarization along $-z$. Instead, we observe a full spin oscillation, which is a signature of coherent spin dynamics. We compare the observed spin texture to 1D GP, Figs. 2(d)–2(f), and 1D LMD, Figs. 2(g)–2(i), predictions.

The two-component GP simulation uses equal interaction strengths between all spin states [19,36], such that all atoms experience the same mean-field effective potential, $V_{\text{eff}} = g\rho$, proportional to the total density. However, the interaction energy can be different for the two spin components, since it depends on the overlap of the spatial wave function with the effective potential. This leads to mean-field-driven spin rotations generated by the difference in interaction energy between matter waves that do and do not interfere (i.e., parallel vs antiparallel spins).

As shown in Fig. 2, the GP simulations capture many details of the observed spin textures. Without interactions, Schrödinger equation (SE) profiles [dashed line in Figs. 2(d)–2(f)] are smooth and positive for small Ω_B . Aside from a small effect due to position-velocity correlations in our system, the SE predicts constant polarization across the cloud, even for larger Ω_B . Interactions drive a spatially varying polarization, including sign changes in S_z and S_y , whose positions are well captured by the GP simulations at various Ω_B .

The LMD model isolates the effective magnetic action of atomic collisions from the complicated density dynamics that occur during reflection of the cloud from the barrier. These calculations use only the average reflected velocity and a static density profile, and thus omit wave packet spreading, density changes due to mean-field kinematics during reflection, as well as velocity-position correlations in predicting the spin texture. Reflected spins traverse the trailing portion of the atomic cloud after reaching the barrier position and experiencing a spin-dependent reflectivity determined by the SE simulation.

As shown in Figs. 2(g)–2(i), the LMD captures the low- Ω_B ($\hbar\Omega_B/2 \ll V_B - E_k$) spin texture, which can be understood as follows. The barrier rotation is a small angle; the first atoms reflected rotate about the incoming $|+x\rangle$ spins. We see from the figure that this results in a sign flip in S_y and two sign flips in S_z (compared to the SE prediction),

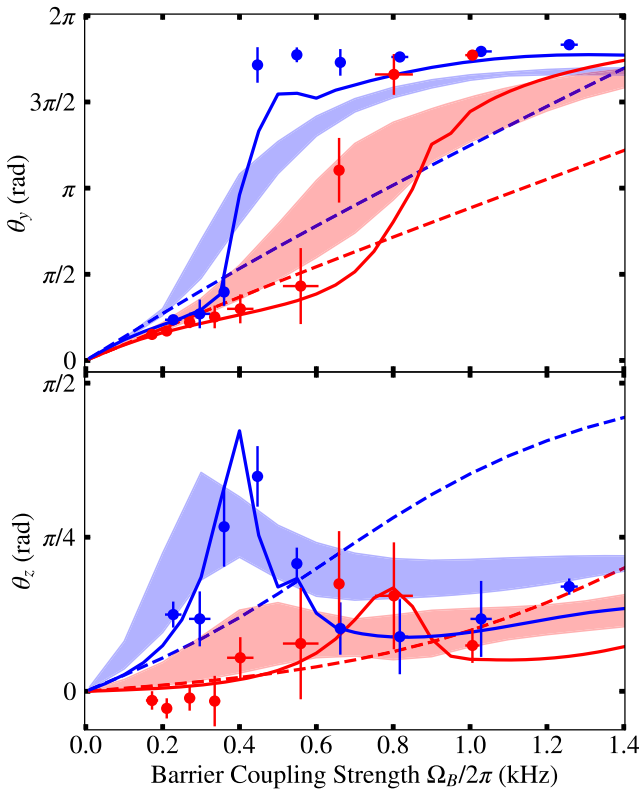


FIG. 3. Net rotation angles of the reflected cloud. Angles of rotation, θ_y (top) and θ_z (bottom), of the reflected atomic cloud for incident wave packets well below the barrier height (red) and near the barrier height (blue). The peak energies of the barriers are 2.25(9) and 1.72(7) kHz in the two cases, while the incident energy of the cloud was 1.61(6) kHz with an rms width of 0.29(3) kHz. Markers represent the measured angles of rotation. Color-coded bands show GP simulations of the experiment, with the shaded regions bounded as in Fig. 2, while the dashed lines indicate SE simulations for the average parameters. The solid curves depict LMD calculations for the average reflected velocity in each scenario.

i.e., a relative phase shift of $\sim\pi$ between the $|+x\rangle$ and $|-x\rangle$ components. This is consistent with a transit time of roughly 10 ms and $\mu/h \sim 50$ Hz. Since the collisions conserve the net magnetization, the integrals of the profiles agree with the SE prediction in the small- Ω_B limit of Fig. 2; this explains the emergence of a spin texture with a sign flip.

Let us now consider the regime of larger Ω_B , where we can no longer make the assumption that the difference between the incident and reflected polarizations is small. Absent atomic interactions, θ_y will continue to precess about the pseudomagnetic field and when $\hbar\Omega_B$ becomes comparable to the energy deficit of the incident particles with respect to the barrier height, θ_z will tend toward $\pi/2$ as the reflected spin becomes polarized along the field direction.

Figure 3 shows θ_y and θ_z measured for variable Ω_B and two barrier heights. We observe that both angles flatten out as a function of Ω_B , in qualitative agreement with the GP and LMD calculations. Once the reflected spin becomes

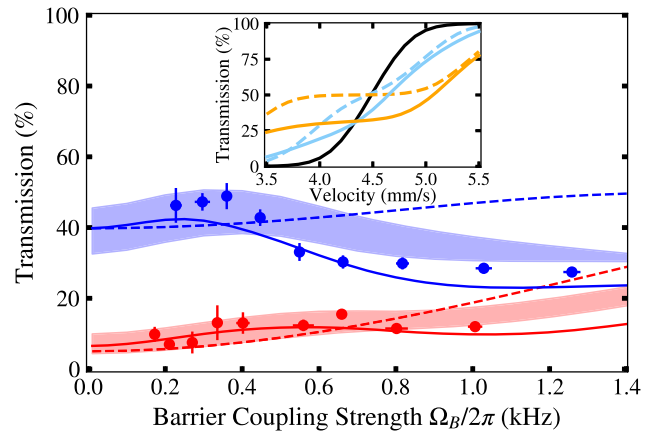


FIG. 4. Effect of spin rotation on transmission. Transmission for the data presented in Fig. 3, color coded as before. Markers display data with statistical error bars, shaded bands illustrate GP simulations bounded as in previous plots, and the dashed lines depict SE simulations for the average experimental parameters. The solid lines indicate LMD calculations averaged over the 0.29 kHz rms energy width of the incident cloud. (Inset) Transmission versus velocity for instances with $\Omega_B/2\pi$ of 0 (black), 1 (blue), and 2 kHz (orange). Dashed lines depict SE simulations, while solid lines represent GP simulations. In the inset, the simulated energy width is 0.18 kHz, narrower than in the experiment to demonstrate the trends clearly.

polarized along $+z$, trailing atoms are driven toward $|+z\rangle$ prior to reflection from the barrier [19]. Thus, above a certain Ω_B , the net spin at the end of the scattering event is largely determined by atomic collisions rather than rotation about the external Ω_B drive. We attribute the discrepancy between the angles at which the dynamics saturate in the models and the experimental data to the precise details of the atomic density during the collision with the barrier that are not captured by the idealized 1D simulations. Note that since the LMD calculation does not incorporate the interactions between atoms at different velocities, it cannot replicate the spatial spin profiles in the large- Ω_B regime where the spin-dependent reflectivity becomes more sensitive to incident energy [19]. Nevertheless, the aggregate angles agree well even at higher Ω_B because they are predominantly set by the total spin rotation atoms acquire while traversing the atomic cloud.

Transmission, shown in Fig. 4, corroborates that spin rotations occur prior to collision with the barrier. When the spin of the trailing portion of the cloud is driven toward $|+z\rangle$, reflection is enhanced because this state experiences an effectively higher barrier. The SE predicts that transmission would tend toward 50% for large Ω_B because all atoms collide with the barrier in $|+x\rangle = (|+z\rangle + |-z\rangle)/\sqrt{2}$. Without atomic interactions, as $|\theta_z| \rightarrow \pi/2$, transmission flattens at 50% over a range of incident velocities, as exhibited in the inset of Fig. 4. Instead, for energies near the barrier height, we observe enhanced

reflection at large Ω_B in qualitative agreement with the simulations incorporating atomic interactions.

Returning to Fig. 3, we note that θ_y and θ_z become Ω_B -insensitive at lower Ω_B for the lower of the two barriers shown. For large energy deficits below the barrier, the time reflected atoms spend inside the barrier is expected to be shorter than for energies closer to the barrier height and hence for fixed Ω_B the rotation angles expected to be smaller in the former case (as indicated by the SE predictions in Fig. 3). This is consistent with previous observations that transmitted particles spend less time interacting with the barrier for lower incident energies [34]. Yet, we do not associate the observed angles with the time reflected atoms spend in the barrier because spin rotations occur prior to interaction with the barrier. While conservation of angular momentum during atomic collisions does preserve the net angles of the cloud, premature rotations cause the spin direction of many atoms entering the barrier to be unknown.

In conclusion, we observe spin dynamics in a two-component BEC with spin-independent interactions. We show that in a counterflow scenario, four-wave mixing gives rise to magnetodynamics. In a mean-field picture, this system behaves as a phase-coherent two-component fluid, and spin rotations are caused by the interaction energy difference between components that do and do not experience interference. This is a new example of a spin-rotation effect for identical spins, closely related to ISRE. In both effects, the spin degree of freedom serves as a distinguishing particle label. In the case of ISRE it is the interaction energy due to particle exchange that is present only for identical spins, while here it is the density fluctuations due to single-particle interference—which also occurs only for identical spins. Their common physical origin is underscored by the fact that in both cases, changing either the particle statistics, bosons \leftrightarrow fermions, or the sign of the interactions, repulsive \leftrightarrow attractive, would reverse the direction of spin rotation [19].

We acknowledge Jeff McGuirk, Dan Stamper-Kurn, Joseph McGowan, Nick Mantella, and Harshil Neeraj for helpful discussions. This work was supported by NSERC, the Fetzer Franklin Fund of the John E. Fetzer Memorial Trust, and AFOSR FA9550-19-1-0365. D. C. S. acknowledges support from the Mitacs Accelerate program. A. M. S. acknowledges support as a fellow of CIFAR.

*Corresponding author: dspierin@mit.edu

[1] A. J. Leggett and M. J. Rice, Spin echoes in liquid He^3 and mixtures: A predicted new effect, *Phys. Rev. Lett.* **20**, 586 (1968); A. J. Leggett, Spin diffusion and spin echoes in liquid ^3He at low temperature, *J. Phys. C* **3**, 448 (1970).

- [2] E. P. Bashkin, Spin waves in polarized paramagnetic gases, *JETP Lett.* **33**, 8 (1981).
- [3] C. Lhuillier and F. Laloë, Transport properties in a spin polarized gas, *J. Phys.* **43**, 197 (1982).
- [4] C. Lhuillier and F. Laloë, Transport properties in a spin polarized gas, *J. Phys.* **43**, 225 (1982).
- [5] B. R. Johnson, J. S. Denker, N. Bigelow, L. P. Lévy, J. H. Freed, and D. M. Lee, Observation of nuclear spin waves in spin-polarized atomic hydrogen gas, *Phys. Rev. Lett.* **52**, 1508 (1984).
- [6] P.-J. Nacher, G. Tastevin, M. Leduc, S. Crampton, and F. Laloë, Spin rotation effects and spin waves in gaseous $^3\text{He} \uparrow$, *J. Phys. Lett.* **45**, 441 (1984).
- [7] W. J. Gully and W. J. Mullin, Observation of spin rotation effects in polarized ^3He - ^4He mixtures, *Phys. Rev. Lett.* **52**, 1810 (1984).
- [8] H. J. Lewandowski, D. M. Harber, D. L. Whitaker, and E. A. Cornell, Observation of anomalous spin-state segregation in a trapped ultracold vapor, *Phys. Rev. Lett.* **88**, 070403 (2002).
- [9] J. M. McGuirk, H. J. Lewandowski, D. M. Harber, T. Nikuni, J. E. Williams, and E. A. Cornell, Spatial resolution of spin waves in an ultracold gas, *Phys. Rev. Lett.* **89**, 090402 (2002).
- [10] X. Du, L. Luo, B. Clancy, and J. E. Thomas, Observation of anomalous spin segregation in a trapped Fermi gas, *Phys. Rev. Lett.* **101**, 150401 (2008); X. Du, Y. Zhang, J. Petricka, and J. E. Thomas, Controlling spin current in a trapped Fermi gas, *Phys. Rev. Lett.* **103**, 010401 (2009).
- [11] F. Piéchon, J. N. Fuchs, and F. Laloë, Cumulative identical spin rotation effects in collisionless trapped atomic gases, *Phys. Rev. Lett.* **102**, 215301 (2009); S. S. Natu and E. J. Mueller, Anomalous spin segregation in a weakly interacting two-component Fermi gas, *Phys. Rev. A* **79**, 051601(R) (2009).
- [12] M. Koschorreck, D. Pertot, E. Vogt, and M. Köhl, Universal spin dynamics in two-dimensional Fermi gases, *Nat. Phys.* **9**, 405 (2013).
- [13] S. Trotzky, S. Beattie, C. Luciuk, S. Smale, A. B. Bardou, T. Enss, E. Taylor, S. Zhang, and J. H. Thywissen, Observation of the Leggett-Rice effect in a unitary Fermi gas, *Phys. Rev. Lett.* **114**, 015301 (2015).
- [14] M. O. Oktel and L. S. Levitov, Internal waves and synchronized precession in a cold vapor, *Phys. Rev. Lett.* **88**, 230403 (2002).
- [15] T. Nikuni, J. E. Williams, and C. W. Clark, Linear spin waves in a trapped Bose gas, *Phys. Rev. A* **66**, 043411 (2002).
- [16] K. Miyake, W. J. Mullin, and P. C. E. Stamp, Mean-field and spin-rotation phenomena in Fermi systems: The relation between the Leggett-Rice and Lhuillier-Laloë effects, *J. Phys.-Paris* **46**, 663 (1985).
- [17] M. O. Oktel and L. S. Levitov, Collective dynamics of internal states in a Bose-Einstein gas, *Phys. Rev. A* **65**, 063604 (2002).
- [18] T. Nikuni and J. E. Williams, Kinetic theory of a spin-1/2 Bose-condensed gas, *J. Low Temp. Phys.* **133**, 323 (2003).
- [19] See Supplemental Material at <http://link.aps.org/supplemental/10.1103/PhysRevLett.132.173401> for additional technical details of the experimental procedure as

- well as further explanation of the GP, SE, and LMD calculations.
- [20] P. Nozieres and D. Saint James, Particle vs. pair condensation in attractive Bose liquids, *J. Phys.* **43**, 1133 (1982).
- [21] E. J. Mueller, T.-L. Ho, M. Ueda, and G. Baym, Fragmentation of Bose-Einstein condensates, *Phys. Rev. A* **74**, 033612 (2006).
- [22] D. S. Hall, M. R. Matthews, C. E. Wieman, and E. A. Cornell, Measurements of relative phase in two-component Bose-Einstein condensates, *Phys. Rev. Lett.* **81**, 1543 (1998).
- [23] E. A. Cornell, D. Hall, M. Matthews, and C. Wieman, Having it both ways: Distinguishable yet phase-coherent mixtures of Bose-Einstein condensates, *J. Low Temp. Phys.* **113**, 151 (1998).
- [24] K. M. Mertes, J. W. Merrill, R. Carretero-González, D. J. Frantzeskakis, P. G. Kevrekidis, and D. S. Hall, Nonequilibrium dynamics and superfluid ring excitations in binary Bose-Einstein condensates, *Phys. Rev. Lett.* **99**, 190402 (2007).
- [25] R. P. Anderson, C. Ticknor, A. I. Sidorov, and B. V. Hall, Spatially inhomogeneous phase evolution of a two-component Bose-Einstein condensate, *Phys. Rev. A* **80**, 023603 (2009).
- [26] M. F. Riedel, P. Böhi, Y. Li, T. W. Hänsch, A. Sinatra, and P. Treutlein, Atom-chip-based generation of entanglement for quantum metrology, *Nature (London)* **464**, 1170 (2010).
- [27] R. Schmied, J.-D. Bancal, B. Allard, M. Fadel, V. Scarani, P. Treutlein, and N. Sangouard, Bell correlations in a Bose-Einstein condensate, *Science* **352**, 441 (2016).
- [28] S. A. Haine, J. Lau, R. P. Anderson, and M. T. Johnsson, Self-induced spatial dynamics to enhance spin squeezing via one-axis twisting in a two-component Bose-Einstein condensate, *Phys. Rev. A* **90**, 023613 (2014).
- [29] T. Laudat, V. Dugrain, T. Mazzoni, M.-Z. Huang, C. L. G. Alzar, A. Sinatra, P. Rosenbusch, and J. Reichel, Spontaneous spin squeezing in a rubidium BEC, *New J. Phys.* **20**, 073018 (2018).
- [30] C. Deutsch, F. Ramirez-Martinez, C. Lacroûte, F. Reinhard, T. Schneider, J. N. Fuchs, F. Piéchon, F. Laloë, J. Reichel, and P. Rosenbusch, Spin self-rephasing and very long coherence times in a trapped atomic ensemble, *Phys. Rev. Lett.* **105**, 020401 (2010).
- [31] M. Egorov, R. P. Anderson, V. Ivannikov, B. Opanchuk, P. Drummond, B. V. Hall, and A. I. Sidorov, Long-lived periodic revivals of coherence in an interacting Bose-Einstein condensate, *Phys. Rev. A* **84**, 021605(R) (2011).
- [32] D. M. Stamper-Kurn and M. Ueda, Spinor Bose gases: Symmetries, magnetism, and quantum dynamics, *Rev. Mod. Phys.* **85**, 1191 (2013).
- [33] R. Ramos, D. Spierings, I. Racicot, and A. M. Steinberg, Measurement of the time spent by a tunnelling atom within the barrier region, *Nature (London)* **583**, 529 (2020).
- [34] D. C. Spierings and A. M. Steinberg, Observation of the decrease of Larmor tunneling times with lower incident energy, *Phys. Rev. Lett.* **127**, 133001 (2021).
- [35] M. Büttiker, Larmor precession and the traversal time for tunneling, *Phys. Rev. B* **27**, 6178 (1983).
- [36] W. Bao, D. Jaksch, and P. A. Markowich, Numerical solution of the Gross-Pitaevskii equation for Bose-Einstein condensation, *J. Comput. Phys.* **187**, 318 (2003).